applied sciences

MDPI

Article

A Comprehensive Method for Calculating Maritime Radar Identification Probability Using 3D Marine Geographical Feature Models

Hao Meng [1], Li-Hua Zhang [1,*], Hai Hu [2], Shi-Jun Rao [3] and Bao-Hui Gao [2]

[1] Department of Military Oceanography and Hydrography & Cartography, Dalian Naval Academy, Dalian 116018, China; menghao0220@foxmail.com
[2] Department of Missile and Warship Gun, Dalian Naval Academy, Dalian 116018, China; searanger@sina.com (H.H.); yerechunfu@foxmail.com (B.-H.G.)
[3] Department of Information System, Dalian Naval Academy, Dalian 116018, China; rsj0207@163.com
* Correspondence: zlhua@163.com

Abstract

To overcome the limitations of existing maritime radar identification analysis methods, which are only applicable to sea-skimming aircraft and fail to quantitatively calculate the probability of radar correctly identifying the target under electromagnetic influence from marine geographical features (MGFs), an advanced method is proposed for calculating the radar identification probability in marine areas using 3D MGF models. The method first established the radar identification criteria in 3D space, considering radar line of sight (LOS), radar target adhesion (RTA), and radar resolutions in range, azimuth angle, and elevation angle. It then comprehensively analyzed errors from both the aircraft and MGFs. Finally, the probability of a target at a specific marine location being correctly identified by radar was calculated using the Monte Carlo method. Theoretical derivations and simulation results demonstrated that: (1) Unlike existing methods limited to sea-skimming aircraft, the proposed method is applicable to aircraft at any altitude, better aligning with current aircraft performance and requirements; (2) While existing methods provide only a binary result of "identified" or "unidentified," the proposed method offers a probability value. For the same marine location point T_a, the proposed method yields radar identification probabilities of 0.0877 for sea-skimming aircraft and 0.5887 for high-altitude aircraft, providing more precise and intuitive decision-making support for mission planners.

Keywords: maritime radar; line of sight; radar target adhesion; marine geographical feature; 3D model; radar resolution; mission planning

check for updates

Academic Editor: Amerigo Capria

Received: 13 June 2025
Revised: 12 July 2025
Accepted: 15 July 2025
Published: 16 July 2025

Citation: Meng, H.; Zhang, L.-H.; Hu, H.; Rao, S.-J.; Gao, B.-H. A Comprehensive Method for Calculating Maritime Radar Identification Probability Using 3D Marine Geographical Feature Models. *Appl. Sci.* **2025**, *15*, 7921. https://doi.org/10.3390/app15147921

Copyright: © 2025 by the authors. Licensee MDPI, Basel, Switzerland. This article is an open access article distributed under the terms and conditions of the Creative Commons Attribution (CC BY) license (https://creativecommons.org/licenses/by/4.0/).

1. Introduction

Radar systems on maritime aircrafts, especially those used for anti-ship missiles, frequently encounter significant detection challenges when the target is close to marine geographical features (MGFs) such as islands and offshore drilling platforms with pronounced electromagnetic characteristics. The challenges arise primarily from two aspects:

(1) The detection blind zones caused by MGFs. MGFs can create physical obstructions that block the radar beam, resulting in areas where the radar cannot detect targets. This is particularly problematic for sea-skimming aircraft when the target is located behind MGFs.

(2) The radar target adhesion (RTA) problem caused by MGFs. Even when the target is within the radar line of sight (LOS), the limitations in radar resolution and the electro-

magnetic interference from MGFs may also lead to the RTA problem. In this case, the target can be mistakenly merged with MGFs and identified as a single target [1].

To address these challenges, current technical research primarily focuses on ensuring that target signals can be detected by radar as well as avoiding the RTA problem. Efforts include improving radar resolution and imaging capabilities [2,3] and developing relevant algorithms [4–14]. While these research directions are theoretically significant, there are still several technical barriers and hardware limitations for their practical application.

From a tactical perspective, optimizing aircraft operations is crucial for overcoming these challenges. This can be achieved by selecting appropriate radar activation points and flight directions to improve the ability of radar correctly identifying the target, even with limited radar resolution and LOS conditions. In this context, several studies have made notable contributions: Hou, Chen, and Dong [15–17] simplified MGFs and targets into point mass models, providing a theoretical basis for evaluating target identification conditions based on radar range and azimuth angle resolution. However, this method can introduce significant errors, especially for complex MGFs like large islands. To address these limitations, based on the 2D contour data of MGFs, Wang [18] attempted to enhance radar's ability to distinguish targets from MGFs by adjusting the aircraft's search direction, and Xie [19] assessed the number of "false targets" that coastlines may generate in a radar system with radar azimuth angle resolution; Wu [20] proposed a strategy to optimize the aircraft's searching direction, ensuring the radar search range covers the target while avoiding MGFs using radar range resolution. Despite these efforts, existing methods still have notable limitations:

(1) They do not account for the influence of MGFs' elevation data and radar elevation angle resolution, limiting their applicability to sea-skimming aircraft and making them unsuitable for advanced high-altitude aircraft;

(2) They ignore potential errors, such as radar activation point errors and MGF position errors. So, they can only provide a binary result of "identified" or "unidentified" and cannot quantitatively calculate the probability of the target being correctly identified by radar at a specific marine location.

With the developments in equipment technology, the usage of advanced high-altitude aircraft is increasing due to their broader field of view, faster speed, and longer range. As for the radar LOS and RTA problems with analysis of high-altitude aircraft in 3D space, it is essential to incorporate the 3D model of MGFs, radar elevation angle resolution, and related errors. Therefore, this paper proposes a method to calculate the radar identification probability (P_{ident}) for a target at a specific marine location. Compared to the existing methods, the proposed method has advantages as follows:

(1) The proposed method further considers the influence of MGFs' elevation data and radar elevation angle resolution, so that it can be applied to aircraft at any altitude, better aligning with the advanced aircraft's performance and requirements.

(2) The proposed method integrates errors from both the MGFs and the aircraft and employs the Monte Carlo method to obtain P_{ident}, instead of the binary result from the existing method, providing more accurate and intuitive decision-making support for the mission planning of maritime aircraft.

2. Principle of Radar Identification Probability Calculation

2.1. Criteria for Radar Identification in 3D Space

As previously discussed, the challenges of radar identification caused by MGFs stem from two main aspects: radar detection blind zones and the RTA problem. To address the former, it is essential to ensure that the target is within the radar LOS. In terms of the RTA problem, it primarily depends on the radar resolution.

Radar resolution can be categorized into range and angular resolutions in the spatial domain. Range resolution refers to the minimum distance between two adjacent targets that the radar can distinguish, primarily determined by the radar signal's bandwidth and pulse width. Angular resolution can be further divided into azimuth angle resolution and elevation angle resolution, which refer to the minimum angles for radar to distinguish two adjacent targets in horizontal and vertical directions, respectively. These are mainly dependent on the radar antenna's beamwidth.

Existing methods [15–20] have mostly simplified MGFs to point masses or relied solely on their 2D contour data, focusing mainly on radar range and azimuth angle resolution within a 2D plane. However, these methods did not fully consider the influence of elevation angle resolution. To extend the research scope from 2D to 3D for advanced high-altitude aircraft, this paper introduces radar elevation angle resolution and an MGF 3D model.

When considering only the spatial domain and ignoring factors such as Doppler resolution, the RTA problem occurs when two or more objects are within the radar LOS and their differences in range, azimuth angle, and elevation angle relative to the radar are all smaller than the respective resolutions.

To more precisely quantify and describe the criteria for the RTA problem in 3D space, this paper establishes a local Cartesian coordinate system with the due north direction as the X-axis, the due east direction as the Y-axis, the instantaneous sea surface as the XOY plane, and the Z-axis pointing vertically upward. Two targets are denoted as the points $T_1(X_{T1}, Y_{T1}, Z_{T1})$ and $T_2(X_{T2}, Y_{T2}, Z_{T2})$, and the radar position is denoted as the point $S(X_S, Y_S, Z_S)$. The schematic diagram of the relative positional relationship between these points is shown in Figure 1.

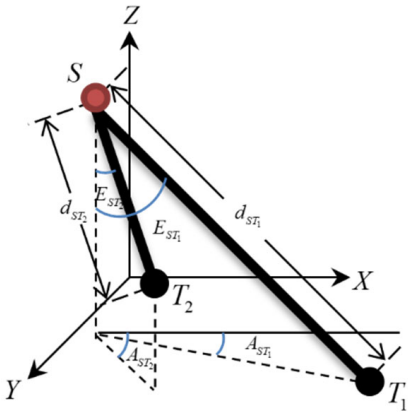


Figure 1. Schematic diagram of the positional relationship between radar and targets.

In Figure 1, d_{ST1} and d_{ST2}, A_{ST1} and A_{ST2}, and E_{ST1} and E_{ST2} represent the distances, azimuth angles and elevation angles from point S to points T_1 and T_2, respectively. According to the definition of RTA, given the radar range resolution R_{res}, azimuth angle resolution A_{res}, and elevation angle resolution E_{res}, when both T_1 and T_2 are within the radar LOS, the condition for the radar to misidentify T_1 and T_2 as a single target is that Equations (1)–(3) are simultaneously satisfied.

$$\left|d_{ST_1} - d_{ST_2}\right| \leq R_{res} \tag{1}$$

$$\left|A_{ST_1} - A_{ST_2}\right| \leq A_{res} \tag{2}$$

$$\left|E_{ST_1} - E_{ST_2}\right| \leq E_{res} \tag{3}$$

The terms in Equations (1)–(3) are as follows:

$$\begin{cases} d_{ST_1} = \sqrt{\left(X_S - X_{T_1}\right)^2 + \left(Y_S - Y_{T_1}\right)^2 + \left(Z_S - Z_{T_1}\right)^2} \\ d_{ST_2} = \sqrt{\left(X_S - X_{T_2}\right)^2 + \left(Y_S - Y_{T_2}\right)^2 + \left(Z_S - Z_{T_2}\right)^2} \\ A_{ST_1} = \arctan\frac{Y_{T_1} - Y_S}{X_{T_1} - X_S} \\ A_{ST_2} = \arctan\frac{Y_{T_2} - Y_S}{X_{T_2} - X_S} \\ E_{ST_1} = \arctan\frac{\sqrt{\left(X_S - X_{T_1}\right)^2 + \left(Y_S - Y_{T_1}\right)^2}}{Z_S - Z_{T_1}} \\ E_{ST_2} = \arctan\frac{\sqrt{\left(X_S - X_{T_2}\right)^2 + \left(Y_S - Y_{T_2}\right)^2}}{Z_S - Z_{T_2}} \end{cases} \tag{4}$$

Therefore, in this paper, the conditions for a target to be correctly identified by the radar are:

(1) The target is within the radar LOS;

(2) If there are any interfering objects within the radar LOS in addition to the target, Equations (1)–(3) are not simultaneously satisfied.

After establishing the radar identification criteria in 3D space, the potential errors from both the MGF and the maritime aircraft are further analyzed in the following section.

2.2. Error Analysis

In addition to the limitations of radar LOS and resolution, potential errors can also affect radar identification. This paper focuses on errors from two sources: the MGF and the maritime radar (aircraft). For MGF data, the errors are mainly due to the accuracy of geospatial surveys. There are planar position errors (ΔX_B, ΔY_B) and elevation data error ΔZ_B. (ΔX_B, ΔY_B) are assumed to follow a 2D normal distribution with independent directions, an expected value of 0, and a standard deviation of σ_{BXY} for both directions. ΔZ_B is assumed to follow a normal distribution with an expected value of 0 and a standard deviation of σ_{BZ}:

$$(\Delta X_B, \Delta Y_B) \sim \mathrm{N}(0, \sigma_{B_{XY}}; 0, \sigma_{B_{XY}}; 0) \tag{5}$$

$$\Delta Z_B \sim \mathrm{N}(0, \sigma_{B_Z}) \tag{6}$$

The errors from the radar (aircraft) mainly stem from the radar system's hardware precision and the navigation errors of the aircraft and its launch platform. They primarily consist of three aspects: the planar position error of the aircraft launch platform (ΔX_L, ΔY_L), the planar position error (ΔX_S, ΔY_S), and the elevation error ΔZ_S of the radar activation point. Similarly, these errors are assumed to follow the normal distributions:

$$(\Delta X_L, \Delta Y_L) \sim \mathrm{N}(0, \sigma_L; 0, \sigma_L; 0) \tag{7}$$

$$(\Delta X_S, \Delta Y_S) \sim \mathrm{N}(0, \sigma_{S_{XY}}; 0, \sigma_{S_{XY}}; 0) \tag{8}$$

$$\Delta Z_S \sim \mathrm{N}(0, \sigma_{S_Z}) \tag{9}$$

To simplify the calculations, this paper combines (ΔX_S, ΔY_S), (ΔX_L, ΔY_L), and (ΔX_B, ΔY_B) as shown in Equation (10), so that ($\Delta X_{S,}$ ΔY_S) can be equivalently considered to follow the 2D normal distribution as shown in Equation (11):

$$\sigma_{m_{XY}}{}^2 = \sigma_{S_{XY}}{}^2 + \sigma_L^2 + \sigma_{B_{XY}}{}^2 \tag{10}$$

$$(\Delta X_S, \Delta Y_S) \sim \mathrm{N}(0, \sigma_{m_{XY}}; 0, \sigma_{m_{XY}}; 0) \tag{11}$$

Similarly, ΔZ_B and ΔZ_S are combined as follows:

$$\sigma_{m_Z}{}^2 = \sigma_{S_Z}{}^2 + \sigma_{B_Z}{}^2 \tag{12}$$

$$\Delta Z_S \sim \mathrm{N}(0, \sigma_{m_Z}) \tag{13}$$

In summary, the errors from both the MGF and the radar (aircraft) are combined and equivalently regarded as the errors of S, whose planar error (ΔX_S, ΔY_S) and elevation error ΔZ_S follow the normal distributions shown in Equations (11) and (13), respectively. Based on that, the actual radar activation point with errors $S'(X_S', Y_S', Z_S')$ and its distribution are shown in Equations (14)–(16), and the schematic diagram of that is shown in Figure 2.

$$\begin{cases} X_S' = X_S + \Delta X_S \\ Y_S' = Y_S + \Delta Y_S \\ Z_S' = Z_S + \Delta Z_S \end{cases} \tag{14}$$

$$(X_S', Y_S') \sim \mathrm{N}(X_S, \sigma_{m_{XY}}; Y_S, \sigma_{m_{XY}}; 0) \tag{15}$$

$$Z_S' \sim \mathrm{N}(Z_S, \sigma_{m_Z}) \tag{16}$$

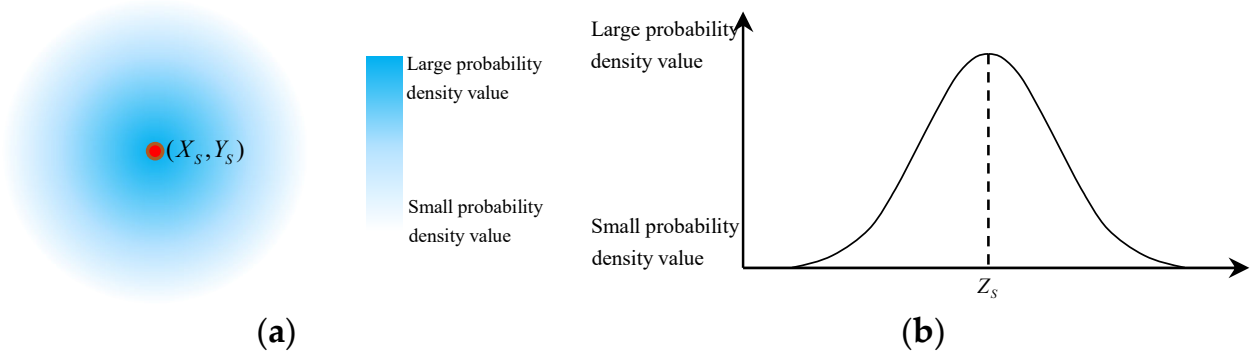


Figure 2. Schematic diagram of the distribution for $S'(X_S', Y_S', Z_S')$. (**a**) Distribution for (X_S', Y_S'); (**b**) Distribution for Z_S'.

In Equations (14)–(16) and Figure 2, $S(X_S, Y_S, Z_S)$ is the theoretical radar activation point.

With the error analysis completed, the detailed steps for calculating the radar identification probability using the Monte Carlo method would be presented.

2.3. Calculation Steps

In this paper, the actual radar operation process is simplified since we paid more attention to the impact of the limitations of radar resolutions and electromagnetic interference from MGFs, and the relevant assumptions are as follows:

Assumption 1. *All objects mentioned in this paper are within the theoretical searching range of the radar.*

Assumption 2. *If the line connecting radar and target is occluded by an MGF, the target would be out of radar LOS and cannot be detected or identified.*

Assumption 3. *If there is no LOS limitation or RTA problem, the target would be correctly identified by the radar, regardless of the dynamic environmental factors, such as sea state or weather.*

Assumption 4. *The result probability P_{ident} only corresponds to the moment when the radar is activated at point S.*

Based on these assumptions, the process of calculating the probability P_{ident} is shown in Figure 3.

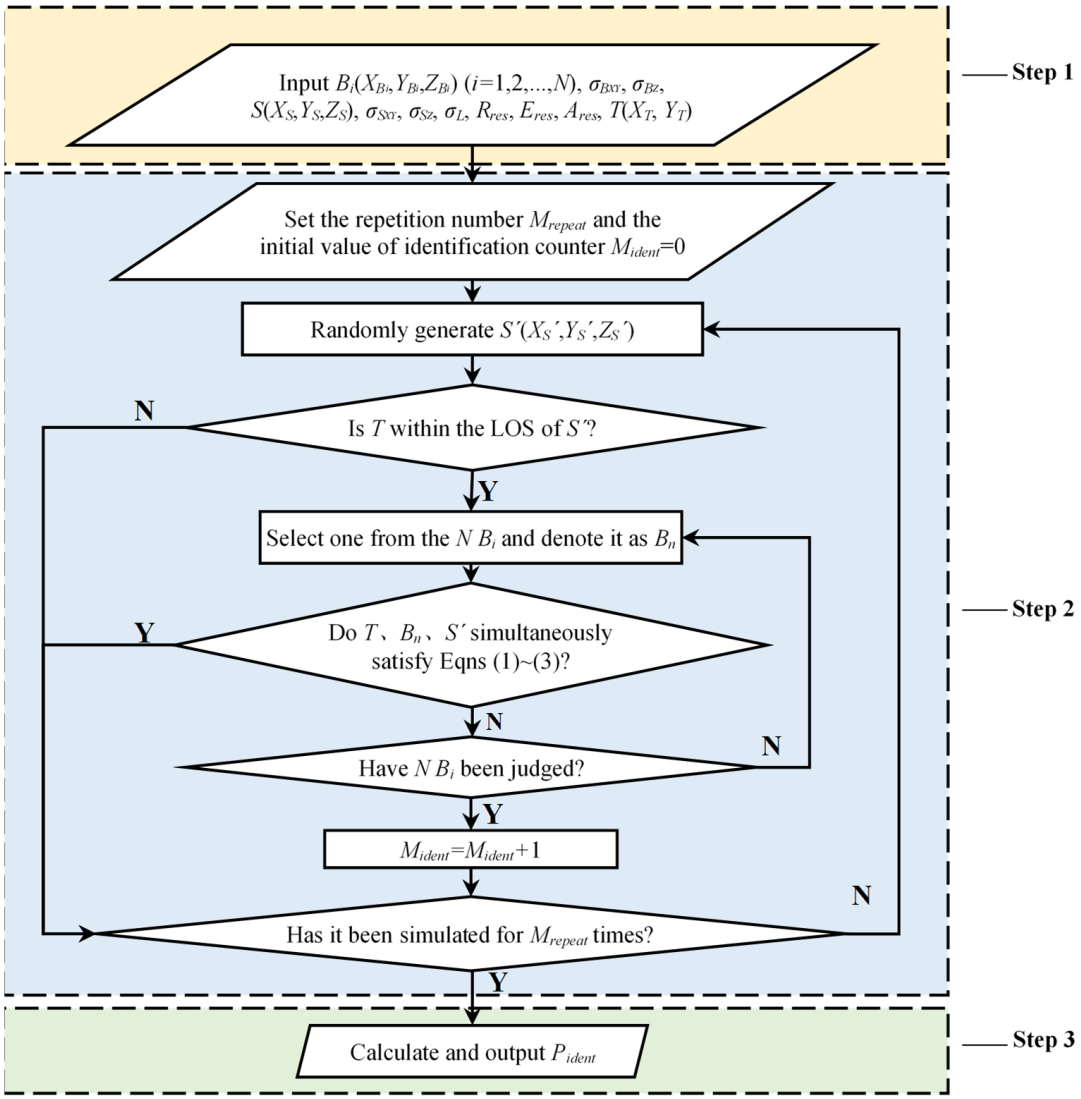


Figure 3. Flowchart of P_{ident} calculation for marine areas.

In Figure 3, the specific implementation process of each step is as follows:

Step 1: Input Data. Based on the 3D model of MGFs, extract the points with pronounced electromagnetic characteristics, denoted as $B_i(X_{Bi}, Y_{Bi}, Z_{Bi})$ (i = 1,2, . . ., N), and input their planar position and elevation error standard deviation σ_{BXY} and σ_{BZ}. According to the aircraft's mission planning and performance parameters, input the radar activation point $S(X_S, Y_S, Z_S)$ and its planar position and elevation error standard deviation σ_{SXY} and σ_{SZ} (for sea-skimming aircraft, Z_S and σ_{SZ} can be set as 0), aircraft launch platform planar position error standard deviation σ_L, radar range resolution R_{res}, elevation angle resolution E_{res}, and azimuth angle resolution A_{res}. Finally, input the marine location point $T(X_T,Y_T)$ where P_{ident} is to be calculated.

Step 2: Monte Carlo Simulation. Set the Monte Carlo repetition times M_{repeat} and initialize the counter M_{ident} = 0. In each simulation:

(1) Randomly generate the radar position point $S'(X_S', Y_S', Z_S')$ based on the theoretical values and errors from Step 1 using Equations (5)–(16).

(2) Determine whether T is within the LOS of S'. If it is, proceed to the next step; otherwise, proceed to the next simulation.

(3) Sequentially determine whether S', T, and each B_i simultaneously satisfy Equations (1)–(3). If none of them satisfies the condition, increment M_{ident} by 1; otherwise, proceed to the next simulation.

Repeat the simulation M_{repeat} times.

Step 3: Calculate P_{ident}. Calculate the ratio of M_{ident} to M_{repeat} to obtain P_{ident}, as shown in Equation (17):

$$P_{ident} = \frac{M_{ident}}{M_{repeat}} \tag{17}$$

Due to the instability of the Monte Carlo method, the accuracy of P_{ident} can be improved by increasing M_{repeat} in Step 2.

By inputting the marine location points around the MGF and repeating the above steps, the distribution of P_{ident} around the MGF can be visually expressed.

3. Simulation and Analysis

3.1. Data Input

To validate the effectiveness and applicability of the proposed method across different scenarios, a series of simulation experiments were conducted. According to the calculation process of P_{ident} shown in Figure 3, the experiment first required the input of data.

To simplify the simulation, it was assumed that all points of the MGF possess pronounced electromagnetic characteristics. Based on this assumption, the experiment used points read from the MGF's stl file as the $B_i(X_{Bi},Y_{Bi},Z_{Bi})$ (i = 1,2, . . ., N) for data input. The stl format is a file format that describes the surface geometry of a 3D object with multiple triangular facets. Its binary format is shown in Table 1.

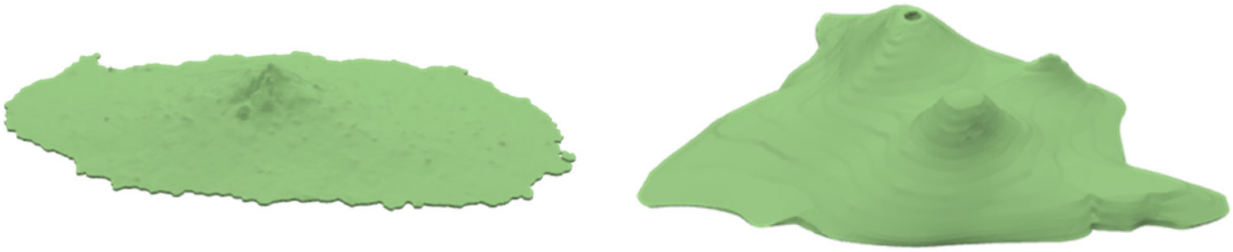
Table 1. stl binary format.

Name	Data Type	Offset/Byte	Notes
Header	String	0	File header
Number of triangles	UInt32	80	Number of triangular facets
Normal vector of triangle M	Single(3)	$50(M-1)+84$	Normal vector of the M-th triangular facet
Vertex1 of triangle M	Single(3)	$50(M-1)+96$	Coordinates of the 1st vertex of the M-th triangular facet
Vertex2 of triangle M	Single(3)	$50(M-1)+108$	Coordinates of the 2nd vertex of the M-th triangular facet
Vertex3 of triangle M	Single(3)	$50(M-1)+120$	Coordinates of the 3rd vertex of the M-th triangular facet
Attribute	UInt16	$50(M-1)+142$	Attribute of the M-th triangular facet

Since the triangular facets of the MGF were obtained using the file format in Table 1, it was accessible to determine whether the marine location point was within the radar LOS by checking whether the line connecting the radar position point and the marine location point intersected with any of the triangular facets. The $B_i(X_{Bi}, Y_{Bi}, Z_{Bi})$ (i = 1, 2, . . ., N) data could be used to determine whether the RTA problem occurred.

Based on that, two islands of different shapes were used as the MGFs for the experiment. The 3D models and parameters of the MGFs are shown in Figure 4 and Table 2.

Since the planar geometric center of the experimental MGFs are close to the coordinate origin, for the convenience of subsequent calculations and explanations, the distance, azimuth angle, and elevation angle between the radar and the coordinate origin are considered as those between the radar and the MGFs for the experiment.



(**a**) (**b**)

Figure 4. 3D models of MGFs for experiment. (**a**) The narrow-shaped island; (**b**) The triangular-shaped island.

Table 2. Parameters of MGFs for experiment.

Parameter	Value of Narrow-Shaped Island	Value of Triangular-Shaped Island	Notes
$[X_{min}, X_{max}]$	[−0.8718 km, 0.9056 km]	[−0.3424 km, 0.6201 km]	The range of MGF along *X*-axis
$X_{max} - X_{min}$	1.7774 km	0.9625 km	The length of MGF along *X*-axis
$[Y_{min}, Y_{max}]$	[−0.5638 km, 0.4370 km]	[−0.5162 km, 0.5892 km]	The range of MGF along *Y*-axis
$Y_{max} - Y_{min}$	1.0008 km	1.1054 km	The length of MGF along *Y*-axis
$[Z_{min}, Z_{max}]$	[0 km, 0.1998 km]	[0, 0.1971 km]	The range of MGF along *Z*-axis
$Z_{max} - Z_{min}$	0.1998 km	0.1971 km	The length of MGF along *Z*-axis
Planar area	1.1220 km^2	0.6582 km^2	The planar area of the MGF under the current tide
Number of facets	74,157	35,080	The number of triangle facets that make up the MGF
Number of vertices	37,988	17,542	The number of points that make up the MGF

In addition to the MGF, the experiment simulated reasonable types of virtual maritime aircraft and the onboard radar. The specific parameters of them and other parameters for the simulation are shown in Table 3.

Table 3. Simulation parameters.

Parameter	Value	Notes
R_{res}	0.5 km	Radar range resolution
A_{res}	1°	Radar azimuth angle resolution
E_{res}	1°	Radar elevation angle resolution
σ_L	0.5 km	Standard deviation of the aircraft launch platform planer position error
σ_{SXY}	0.1 km	Standard deviation of the radar activation point planer position error
σ_{SZ}	0.01 km for high-altitude aircraft 0 km for sea-skimming aircraft	Standard deviation of the radar activation point elevation error
σ_{BXY}	0.5 km	Standard deviation of the MGF planer position error
σ_{BZ}	0.005 km	Standard deviation of the MGF elevation error

Note: All values in the table are hypothetical.

To verify the applicability of the proposed method to aircraft at any altitude, three groups of radar position points were constructed, as shown in Table 4.

Table 4. Radar positions.

Group	Point Name	X_S /km	Y_S /km	Z_S /km	Aircraft State	Relative Positional Relationship with the MGFs for Experiment		
						Elevation Angle/°	Azimuth Angle/°	Distance /km
①	S_1	18	0	0.01	Sea-skimming	0	0	18
	S_2	15	0	10	High-altitude	34		
②	S_3	0	18	0.01	Sea-skimming	0	90	
	S_4	0	15	10	High-altitude	34		
③	S_5	12.7	12.7	0.01	Sea-skimming	0	45	
	S_6	10.5	10.5	10	High-altitude	34		

3.2. Result Calculation

With M_{repeat} set to 10,000 and the input data from Section 3.1, we calculated and visualized the P_{ident} distribution around the MGFs for the experiment under the radar points from S_1 to S_6. The results are shown in Figures 5 and 6.

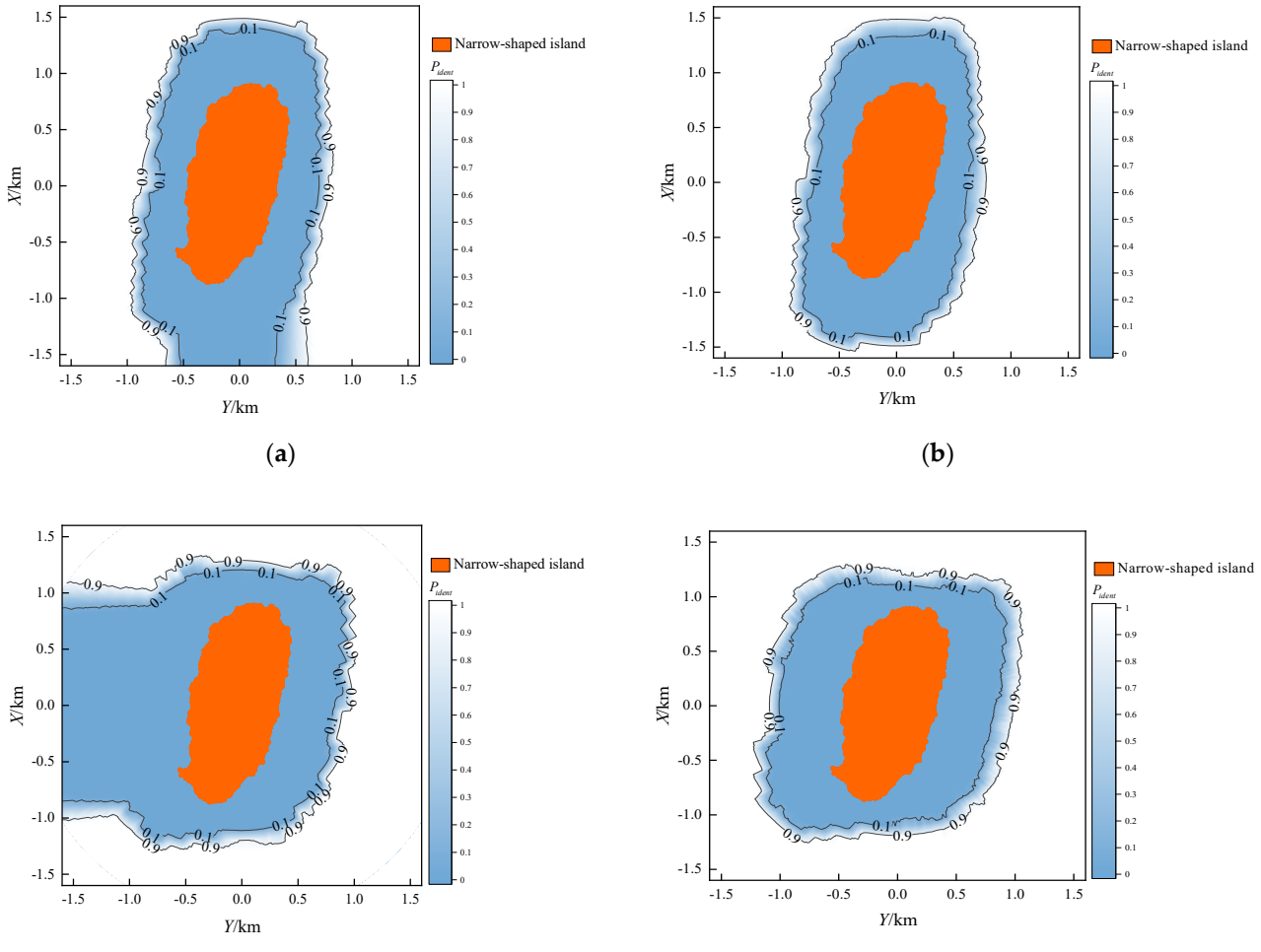
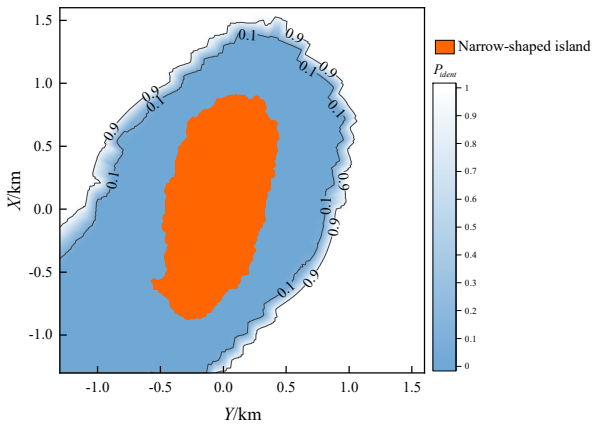
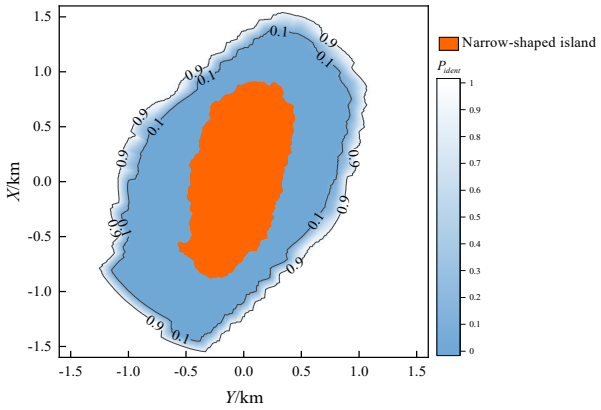


Figure 5. *Cont.*

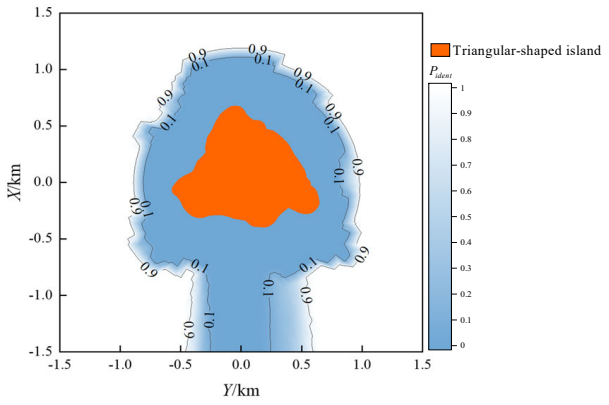


(**e**)

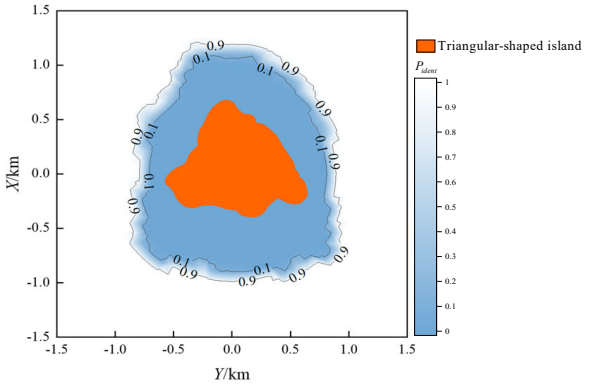


(**f**)

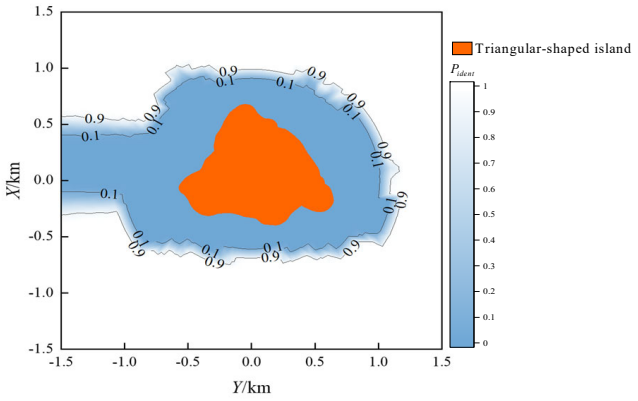
Figure 5. Distribution of P_{ident} in marine areas under different radar positions for the narrow-shaped island. (**a**) When regarding S_1 as radar position (sea-skimming); (**b**) When regarding S_2 as radar position (high-altitude); (**c**) When regarding S_3 as radar position (sea-skimming); (**d**) When regarding S_4 as radar position (high-altitude); (**e**) When regarding S_5 as radar position (sea-skimming); (**f**) When regarding S_6 as radar position (high-altitude).



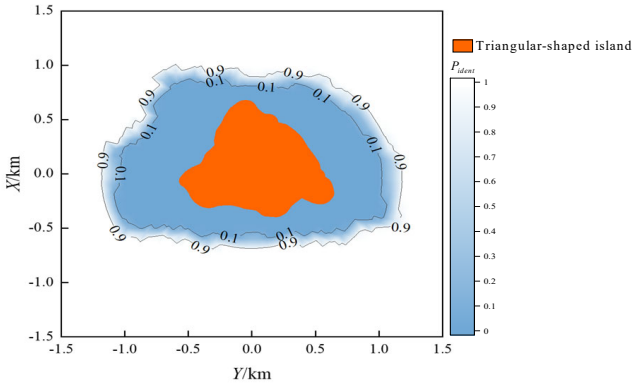
(**a**)



(**b**)

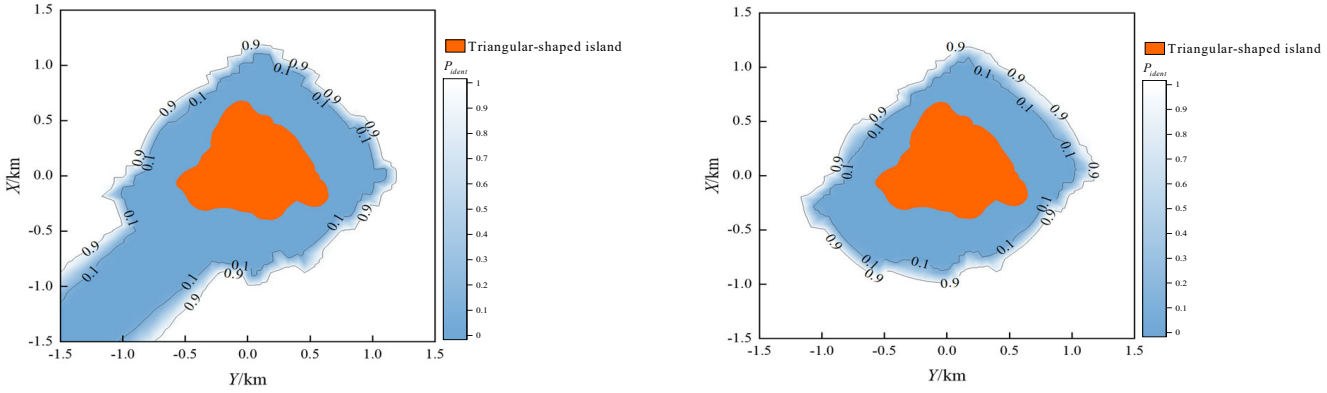


(**c**)



(**d**)

Figure 6. *Cont*.



(**e**) (**f**)

Figure 6. Distribution of P_{dist} in marine areas under different radar positions for the triangular-shaped island. (**a**) When regarding S_1 as radar position (sea-skimming); (**b**) When regarding S_2 as radar position (high-altitude); (**c**) When regarding S_3 as radar position (sea-skimming); (**d**) When regarding S_4 as radar position (high-altitude); (**e**) When regarding S_5 as radar position (sea-skimming); (**f**) When regarding S_6 as radar position (high-altitude).

3.3. Result Analysis

For ease of description, in this paper, the marine areas around the MGF for the experiment were denoted as different levels according to their value of P_{ident} as shown in Table 5.

Table 5. Marine area level.

Value of P_{ident}	Level of Region
$P_{ident} < 0.1$	Level I
$0.9 \geq P_{ident} \geq 0.1$	Level II
$P_{ident} > 0.9$	Level III

As illustrated in Figures 5 and 6, the proposed method effectively calculates and visualizes the P_{ident} distribution around the MGFs for both sea-skimming and high-altitude scenarios.

Combining Figures 5 and 6 and Table 4, it can be observed that, the Level I and II regions always mirror the MGF's outline but are stretched along the radar's azimuth bearing. For example, when the radar is north of MGFs (0° azimuth) in Figures 5b and 6b, the Level I and II regions extend along the *X*-axis as "enlarged copies" of both narrow-shaped island and triangular-shaped island; when radar moves east (90° azimuth) in Figures 5d and 6d, they lengthen along the *Y*-axis. These are consistent with physical expectations and provide an initial validation of the proposed method.

Furthermore, Given the same distance and azimuth angle between the MGF and the radar, the changes in elevation angle caused by the decrease in Z_S (from high-altitude to sea-skimming) also result in the shapes of the Level I and Level II regions extending towards the azimuth direction of the aircraft. This indicates that the threat level of the marine areas around the MGF is enhanced, consistent with the radar detection blind zones caused by MGF occlusion for sea-skimming aircraft, further demonstrating the effectiveness of the proposed method in this paper.

In addition to the overall result, we selected marine location points T_a (0.6 km, −0.8 km) for the narrow-shaped island and T_b (0.6 km, −0.6 km) for the triangular-shaped island as

individual cases since they were always within the LOS of radar at the point of S_1, S_2, S_5, and S_6. The corresponding probabilities were extracted and shown in Table 6.

Table 6. P_{ident} of T_a and T_b under different radar position points.

Point Name	Aircraft State	P_{ident} at T_a with the Interference of Narrow-Shaped Island	P_{ident} at T_b with the Interference of Triangular-Shaped Island
S_1	Sea-skimming	0.9564	0.0505
S_2	High-altitude	0.9990	0.3833
S_5	Sea-skimming	0.0877	0.9625
S_6	High-altitude	0.5887	0.9997

From Table 6, it can be seen that, even for T_a and T_b which always satisfied the radar LOS condition, changes in the aircraft state still have a significant impact on P_{ident}. For S_5 and S_6, under the interference of the narrow-shaped island, the change in aircraft state from sea-skimming to high-altitude increased the P_{ident} of T_a by 0.5010; for S_1 and S_2, under the interference of the triangular-shaped island, the change in aircraft state from sea-skimming to high-altitude increased the P_{ident} of T_b by 0.3328. This indicates the importance of introducing the radar elevation angle resolution and MGF 3D model, and the necessity of the proposed method.

3.4. Practical Application

In actual application scenarios, the complex relationship between radar activation point, MGF data, and P_{ident} is further compounded by dynamic maritime environment, aircraft performance, and specific mission requirement. Owing to the non-linear interaction among these factors, analytically determining the single optimal radar activation point, either by maximizing P_{ident} at a given target location or by minimizing the combined extent of Level I and Level II regions, is computationally intractable and often operationally impractical.

The proposed method circumvents this difficulty by providing planners with an explicit, probability-based comparison of candidate configurations. The Inputs consist of

(1) The 3D MGF model;
(2) The area around the MGF whose P_{ident} needs be calculated;
(3) Radar resolution parameters;
(4) Errors mentioned in Section 2.2;
(5) A discrete set of candidate radar activation points that satisfy the constraints.

The proposed method would then return the corresponding P_{ident} values, and the mission planners can select the most operationally suitable radar activation point from candidates without recourse to exhaustive numerical optimization.

Example. Consider the narrow-shaped island scenario with two candidate radar activation points S_2 and S_6 due to the constraints. If surveillance intelligence indicates that a target is expected at location T_a, and the computed probabilities are $P_{ident}(S_2) = 0.9990$ and $P_{ident}(S_6) = 0.5887$. The planner therefore selects S_2, achieving a substantial increase in identification confidence.

3.5. Result Comparison

To compare the results from the proposed method and existing methods, we first need to clarify the calculation principle of the existing methods. Existing methods predominantly utilize the 2D contour data of MGFs and are limited to sea-skimming aircraft. These methods do not account for potential errors and merely provide a binary result of "identified" or "unidentified" rather than a probability of identification. The relevant calculation is based

on the 2D contour data of MGFs, using the LOS condition and Equations (1) and (2), while neglecting the impact of radar elevation angle resolution (Equation (3)). As these methods do not incorporate error considerations, there is no requirement for Monte Carlo simulation.

To further illustrate the differences between the proposed method and existing methods, we selected radar position points S_1, S_3, and S_5 as examples (sea-skimming aircraft), and calculated and visualized the binary result surrounding the narrow-shaped island. The comparison of these results with those obtained from the proposed method is shown in Figure 7.

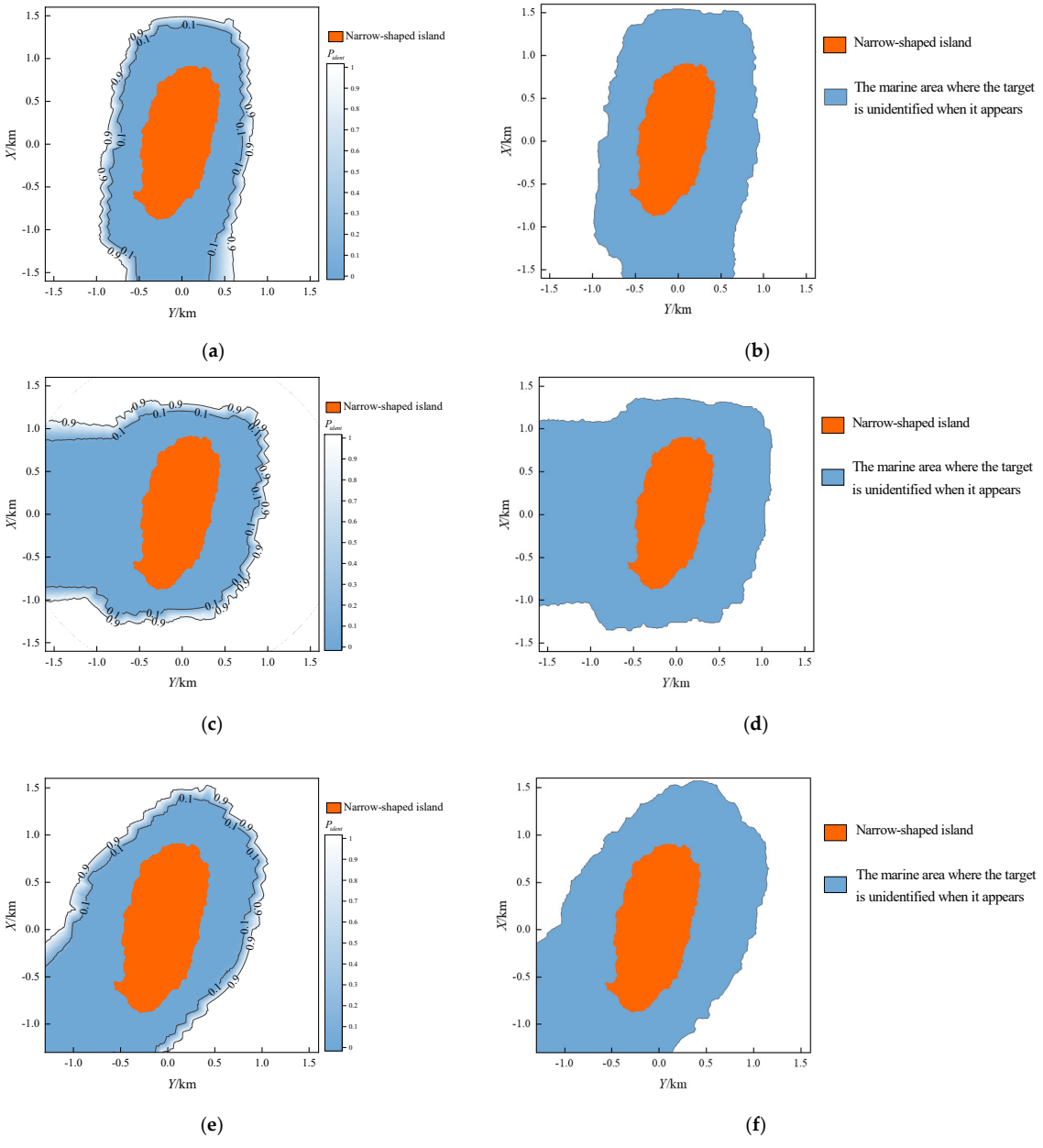


Figure 7. Comparison of results from two methods. (**a**) Probability result of proposed method (When regarding S_1 as radar position); (**b**) Binary result of existing method (When regarding S_1 as radar position); (**c**) Probability result of proposed method (When regarding S_3 as radar position); (**d**) Binary result of existing method (When regarding S_3 as radar position); (**e**) Probability result of proposed method (When regarding S_5 as radar position); (**f**) Binary result of existing method (When regarding S_5 as radar position).

From Figure 7, it can be seen that the shape and area of the "unidentified" region from existing methods is similar to those of the sum of Level I and Level II regions from the proposed method, which validates the effectiveness of the proposed method from a different angle.

Besides that, the proposed method not only can be applied to aircraft at any altitude, but it can also take more errors into consideration, and the probability result rather than the binary result provides more precise and intuitive decision-making support for aircraft mission planners.

The detailed comparison between the proposed method and the existing methods in terms of RTA determination conditions, MGF data utilization, and other factors is shown in Table 7.

Table 7. Comparison of two methods.

Method	RTA Determination Factors	MGF Data Utilization	Applicable Range	Error Consideration	Result
Existing methods	Range resolution Azimuth angle resolution	2D contour	Sea-skimming aircraft	No	Binary
Proposed method	Range resolution Azimuth angle resolution Elevation angle Resolution	3D model	Aircraft at any altitude	Yes	Probability

In summary, the proposed method, which incorporates radar elevation angle resolution and the MGF 3D model, is applicable to aircraft at any altitude in 3D space. It can quantitatively calculate the probability of radar correctly identifying a target at a specific marine location, providing more precise and intuitive decision-making support for aircraft mission planners. Compared with existing methods, it better aligns with the current performance and requirements of aircraft.

4. Conclusions

Based on theoretical derivation and simulation analysis, the conclusions are as follows:

(1) In contrast to existing methods limited to sea-skimming aircraft, the proposed method offers a significant advancement by being applicable to aircraft at any altitude.

(2) With the input parameters, the proposed method can effectively calculate the probability P_{ident} of the target closed to MGF being correctly identified by the radar, rather than a binary result of "identified" or "unidentified" from existing methods, which helps provide more precise and intuitive decision-making support for aircraft mission planners.

However, we acknowledge that our current model does not account for dynamic environmental factors such as sea state or weather conditions, nor does it consider the correlations between the mentioned errors. Future work will focus on incorporating these elements to enhance model accuracy and robustness. Specifically, we plan to analyze error correlations to refine our method, which means that the distribution for actual radar activation point $S'(X_S', Y_S', Z_S')$ would consider the covariances between MGFs and aircraft caused by dynamic environmental factors, and each Monte Carlo simulation would then sample from this refined distribution, yielding more accurate and robust probability results.

Author Contributions: Conceptualization, H.M. and L.-H.Z.; methodology, H.M. and L.-H.Z.; validation, H.H., S.-J.R. and B.-H.G.; formal analysis, H.M.; writing—original draft preparation, H.M.; writing—review and editing, L.-H.Z.; visualization, H.M. All authors have read and agreed to the published version of the manuscript.

Funding: This research received no external funding.

Institutional Review Board Statement: Not applicable.

Informed Consent Statement: Not applicable.

Data Availability Statement: The original contributions presented in this study are included in the article. Further inquiries can be directed to the corresponding author.

Conflicts of Interest: The authors declare no conflicts of interest.

Abbreviations

The following abbreviations are used in this manuscript:

MGF	marine geographical feature
LOS	line of sight
RTA	radar target adhesion

References

1. Liu, C.; Wang, Y.J. Review of multi-target tracking technology for marine radar. *J. Radars* **2021**, *10*, 100–115.
2. Deng, Y.K.; Yu, W.D.; Wang, P.; Xiao, D.J.; Wang, W.; Liu, K.Y. The High-Resolution Synthetic Aperture Radar System and Signal Processing Techniques: Current progress and future prospects [Review Papers]. *IEEE Geosci. Remote Sens. Mag.* **2024**, *12*, 169–189. [CrossRef]
3. Teng, L.; Liang, Z.N.; Liu, Q.H. Advanced technology of high-resolution radar: Target detection, tracking, imaging, and recognition. *Sci. China Inf. Sci.* **2019**, *62*, 40301. [CrossRef]
4. Feng, L.; Duan, Z.S.; Yuan, X.H. Error bounds for joint detection and estimation of multiple unresolved target-groups. *Digit. Signal Process.* **2016**, *51*, 10–24. [CrossRef]
5. Liu, W.F.; Zhu, S.J.; Wen, C.L. Structure modeling and estimation of multiple resolvable group targets via graph theory and multi-bernoulli filter. *Automatica* **2018**, *89*, 274–289. [CrossRef]
6. Chen, J.; Du, L.; Guo, G.B.; Yin, L.W.; Wei, D. Target-attentional CNN for Radar Automatic Target Recognition with HRRP. *Signal Process.* **2022**, *196*, 108497. [CrossRef]
7. Jiang, W.; Wang, Y.P.; Li, Y.; Lin, Y.; Shen, W.J. Radar Target Characterization and Deep Learning in Radar Automatic Target Recognition: A Review. *Remote Sens.* **2023**, *15*, 3742. [CrossRef]
8. Rizvi, S.M.D.; Ahmad, S.; Khan, K.; Hasan, A.; Masood, A. Deep Learning Approach for Fixed and Rotary-Wing Target Detection and Classification in Radars. *IEEE Aerosp. Electron. Syst. Mag.* **2022**, *37*, 32–42. [CrossRef]
9. Zhao, L.F.; Wang, L.; Yang, L. The race to improve radar imagery: An overview of recent progress in statistical sparsity-based techniques. *IEEE Signal Process. Mag.* **2016**, *33*, 85–102. [CrossRef]
10. Liu, Z.W.; Chen, Y.; Lu, Y.B. PHD filter for small-angle crossing of multi-target trajectories. *Syst. Eng. Electron.* **2023**, *45*, 982–990.
11. Shi, D.Y.; Lin, Q.; Hu, B. Review on applications of deep learning in radar target detection. *Radar Sci. Technol.* **2022**, *20*, 589–605.
12. Rathod, S.; Sreenivasulu, K.; Beenamole, K.S.; Ray, K.P. Evolutionary trends in Transmit/Receive Module for Active Phased Array Radars. *Def. Sci. J.* **2018**, *68*, 553–559. [CrossRef]
13. Justin Sagayaraj, M.; Jithesh, V.; Singh, J.B.; Roshani, D.; Srinivasa, K.G. A Hybrid Approach to Cognition in Radars. *Def. Sci. J.* **2018**, *68*, 183–189. [CrossRef]
14. Kang, Z.; Ma, F.; Chen, C.; Sun, J. YOSMR: A Ship Detection Method for Marine Radar Based on Customized Lightweight Convolutional Networks. *Mar. Sci. Eng.* **2024**, *12*, 1316. [CrossRef]
15. Hou, X.L.; Chen, R.; Chen, D.A. Research on distance and angle to turn on terminal guidance radar of ASM attacking ship of formation in coral islands or reefs area. *Command Control Simul.* **2017**, *39*, 76–80.
16. Chen, R.; Shen, P.Z.; Zhang, H.F. Research on terminal guidance radar starting distance and angle of ASM attacking island area ship. *J. Proj. Rocket. Missiles Guid.* **2016**, *36*, 5–8.
17. Dong, F.; Ouyang, Z.H.; Liu, W.B. An algorithm for determining the terminal guidance starting point of anti-ship missile. *J. Proj. Rocket. Missiles Guid.* **2019**, *39*, 139–142.

18. Wang, P.Y.; Gao, R.; Wang, Y.N. Search course optimization of air-to-ship missile under the reef environment. *J. Nav. Aeronaut. Astronaut. Univ.* **2020**, *35*, 395–399.
19. Xie, Y.P.; Li, M.; Wang, G.H. Research on anti-ship missile acquire target sailing along coast. *Tactical Missile Technol.* **2018**, *6*, 52–56.
20. Wu, S.; Xie, C.S.; Li, J.J. Based on GIS the search strategy of anti-ship missile terminal guidance radar near the offshore. *J. Ordnance Equip. Eng.* **2019**, *40*, 98–101.

Disclaimer/Publisher's Note: The statements, opinions and data contained in all publications are solely those of the individual author(s) and contributor(s) and not of MDPI and/or the editor(s). MDPI and/or the editor(s) disclaim responsibility for any injury to people or property resulting from any ideas, methods, instructions or products referred to in the content.